Analyst

PAPER

View Article Online
View Journal | View Issue

Cite this: *Analyst*, 2016, **141**, 4659

An array of individually addressable micro-needles for mapping pH distributions†

Claudio Zuliani,*[a] Fu Siong Ng,[b] Andrea Alenda,[a] Amir Eftekhar,[a] Nicholas S. Peters[b] and Christofer Toumazou[a]

Received 17th March 2016,
Accepted 11th May 2016

DOI: 10.1039/c6an00639f

www.rsc.org/analyst

This work describes the preparation of an array of individually addressable pH sensitive microneedles which are sensitized by electrodepositing iridium oxide. The impact of the deposition potential, storage conditions and interferents on the sensor characteristics such as slope, offset, intra- and inter-batch reproducibility is investigated. The device may be a useful tool for carrying out direct pH measurements of soft and heterogeneous samples such as tissues and organs. For example, we demonstrated that the microneedle array can be employed for real-time mapping of the cardiac pH distribution during cycles of global ischemia and reperfusion.

Introduction

Microneedle arrays have demonstrated a huge potential in biomedical applications such as for minimally invasive therapeutic delivery of vaccines and hormones as well as for the detection of metabolites, therapeutic drugs and disease biomarkers in transdermal fluids.[1–15] Silicon has been used predominantly for fabrication of microneedles, however the fragility and the cost of the microfabrication process are major drawbacks for this material.[1–4] Injection molding has instead emerged as an alternative fabrication process offering advantages such as cost and robustness.[16,17] Microneedles can offer minimally invasive tools in the field of analytical science for example in order to achieve high-density chemical mapping, thus to measure chemical heterogeneities in biological systems such as in tissues and organs.

In this regard, pH measurement is rather complicated to obtain since the glass-type pH electrode cannot often be applied in biomedical and physiological research because of the cumbersome miniaturisation and sensor format, *e.g.*, not conformal to organs.[18–21] In addition, an array of pH sensors provides a better mapping of tissues or organs than a single-spot device because of possible heterogeneities across different sites and along the depth of the sample.[22,23] In this regard, it is important to note that the fabrication of an array from glass-type pH electrodes is a difficult process. Among materials that have emerged as alternatives to the glass electrode, iridium oxide (IrOx) is a possible candidate since it exhibits high sensitivity in a wide pH range, rapid response times, good chemical selectivity and ease of miniaturization.[24,25] Iridium oxide electrodes exhibit a super-Nernstian response of 65–80 mV per pH unit depending on preparation and discussions on the complex equilibrium interfacial reactions that account for this behaviour can be found elsewhere.[18,24–26]

An example of heterogeneous pH variation is the setting of myocardial ischemia due to a switch towards anaerobic metabolism and the development of lactic acidosis.[27–32] Reperfusion of the ischemic myocardium[33] leads to a rapid restoration of pH to pre-ischemic values,[34,35] which may in part contribute towards reperfusion injury.[36–38] In this context, mapping pH distribution complements the physiological profile offered by electrograms and highlights spatially heterogeneous biochemical changes predisposing to ischemia- and reperfusion-induced arrhythmias.[27,31,32,39] Optical mapping using pH fluorescent indicators is possible, however, there are several drawbacks such as limited temporal resolution, phototoxicity during prolonged illumination, scale of the map (microscopic rather than macroscopic) and cost.

This work reports on the preparation of an array of individually addressable iridium-oxide coated microneedles fabricated from a plastic substrate obtained by injection moulding. This device may afford a novel low-cost bio-analytical tool suitable for high-density spatial mapping of pH in solid soft samples such as organs and tissues. The needles were inserted into an explanted perfused rat heart and employed for real-time mapping of the pH distribution across several sites of the whole organ during cycles of ischemia/reperfusion.

[a]*Centre for Bioinspired Technology, Electrical and Electronic Engineering Department, Imperial College London, South Kensington, London, UK. E-mail: c.zuliani@imperial.ac.uk*
[b]*National Heart & Lung Institute, Imperial College London, London, UK*
†Electronic supplementary information (ESI) available. See DOI: 10.1039/c6an00639f

Experimental

Chemicals & materials

Buffer salts (pH 4, 5, 6, 7, 8), KCl, NaCl, KNO_3, Na_2HPO_4, NaH_2PO_4, $MgCl_2$, $CaCl_2$, $NaHCO_3$, glucose, K_3IrCl_6, K_2CO_3, and oxalic acid were from Sigma-Aldrich, UK. N_2 (99.9%) and the O_2/CO_2 mixture (95/5) were from BOC, UK. 75 and 500 μm Mylar sheets, double adhesive tape, silver-loaded epoxy resin and Araldite epoxy resin were from Farnell, UK. Insulated stainless steel wires (125 μm conductor and 25 μm thick Teflon® insulation) were from Advent Materials, UK. PET microneedle arrays were fabricated by injection molding (PEP, France).

Equipment

Gold was sputtered using a sputter-coater (Quorum Technologies, UK). Ivium Compact (Alvatek, UK) with the 32-channel probe, WE32 module, was employed for the simultaneous electrochemical deposition of iridium oxide using an Ag/AgCl electrode (IJ Cambria, UK) and a coiled 0.5 mm Pt wire (Advent Metals, UK) as reference and counter electrodes, respectively. A salt-bridge containing aqueous 0.5 M H_2SO_4 was employed while recording voltammograms of the IrOx coated electrodes immersed in 0.5 M H_2SO_4. The potentiometric traces of the pH sensors were recorded under quiescent conditions using the EMF-16 high-input impedance voltmeter (Lawson, USA) and a double junction Ag/AgCl reference electrode (Sigma-Aldrich, UK) filled with an inner solution of 4.0 M KCl and an outer solution of 1.0 M KNO_3. It should be noted that employing a double junction Ag/AgCl and using the same buffer for bathing and perfusing the heart minimizes the contribution of the junction potentials across the phase boundaries. The pH of all the solutions was measured using a pH meter from Hanna (Sigma-Aldrich, UK). A caliper was employed to measure the height of the needles and distances between them. The heart slices were imaged with a Zeiss Axio Observer wide-open field microscope following histopathological treatment. The electrocardiogram (ECG) was monitored throughout the *ex vivo* experiment using a LabChart and a bioamplifier (both AD Instruments, New Zealand). Plastic and adhesive sheets were laser-micromachined in order to produce a mask for the microneedle array. Deionized (DI) water with a resistivity of 18.2 MΩ cm was obtained with a water purification system (Purite, UK) and it was used for making aqueous solutions. A pneumatically-actuated inserter (Blackrock, USA) with a 1.0 mm piston was employed to insert the microneedle array into the heart.

Procedures

Fig. S1† describes the steps followed for patterning gold on the surface of the substrate. In practice, a 500 μm thick Mylar® sheet was laser-cut in order to pattern gold by means of a sputter-coater. Following this step, a 75 μm thick Mylar® sheet laminated together with a double adhesive tape was laser-cut and laid onto the microneedle in order to leave only the needles and the conductive pads exposed. 10 cm long insulated stainless steel was cut from the reel and the insulator was gently scraped from both ends using a scalpel blade. The wires were then individually glued to the gold conductive pads of the microneedle array platform using silver epoxy resin. After 24 hours curing, these joints and the remaining part of the conductive pads were electrically insulated using epoxy resin. Iridium oxide (IrOx) was electrochemically deposited onto the gold microneedles using a slight modification of a previously reported protocol.[40,41] In practice, 62.7 mg of K_3IrCl_6 were dissolved in 30 mL of deionized water, then 87.0 mg of oxalic acid were added to the mixture followed by 331.7 mg of K_2CO_3. The mixture was stirred at 800 rpm and heated up using a water bath maintained at 60 °C. The solution turned pale yellow from yellow after 1 hour, and after 5–6 hours it became transparent. After this time, the mixture was removed from the heat and left stirring overnight using an Al foil to protect it from direct sunlight. The solution turned pale purple/blue after this 24 hours protocol.

The final mixture was stored at 4 °C but a slow change in colour from pale purple/blue to intense blue occurred over time (30–60 days). Nevertheless, the solution thus prepared could be used for the IrOx electro-deposition for up to 2 months with reproducible results. Plating of IrOx was obtained under quiescent conditions by applying a constant potential for 600 seconds. It has been suggested that the oxalate ligand is oxidized to form CO_2 during the deposition leading to the deposition of a hydrated form of iridium oxide[18] although other mechanisms have been proposed.[25] After plating, a dark blue deposit could be observed on the area of the needle array which was then rinsed using DI water and then dried by blowing air before being stored in Petri dishes. The devices were calibrated by measuring the potential bias, ΔE, between each individual IrOx-coated needle (pH sensor) against the reference electrode. The ΔE was calculated as the average of values over a 3 minutes measurement with the device dipping into the given buffer. The drift of the sensor was evaluated by monitoring the potential in a phosphate buffer having a pH equal to 6.80 ± 0.05 and composed of an equimolar (10 mM) solution of Na_2HPO_4 and NaH_2PO_4 in 0.1 M aqueous KCl or KNO_3.

Biological protocols

All studies were approved by the institutional animal care and use committee of Imperial College London. Tyrode's solution was freshly prepared and consisted of (in mM): 128.2 NaCl, 4.7 KCl, 1.19 NaH_2PO_4, 1.05 $MgCl_2$, 1.3 $CaCl_2$, 20.0 $NaHCO_3$, 11.1 glucose and was gassed with an O_2/CO_2 mixture (95 : 5). Explanted hearts (n = 3) were obtained from male Wistar rats that had been anesthetized with isoflurane prior to sacrifice by rapid manual cervical dislocation, in line with Schedule 1 of the Animals (Scientific Procedures) Act 1986. The heart was rapidly excised and arrested in cold Tyrode's solution. The heart was then subsequently perfused *via* the aorta and superfused with oxygenated Tyrode's solution maintained at 37 °C. Mean coronary arterial pressure was maintained at 60 mmHg. The pH of the buffer in which the heart bathed was equal to

7.40 ± 0.10. A two-point calibration using buffer solutions of pH equal to 4 and 8 was carried out prior to the experiment in order to determine the value of the slope. Following this, a double junction Ag/AgCl reference electrode and the IrOx-coated microneedle array were immersed into the Tyrode's solution in which the heart bathed. A one-point calibration was carried out in this media in order to recalculate the offset value. This one-point calibration was repeated at the very end of the ischemia/reperfusion experiment after removing the needles from the heart and repositioning them into the Tyrode's buffer. This procedure corrects for the drift due to the biofouling of the sensors occurring during the experiment. A linear correction for the drift was applied, *i.e.*, the offset value changes linearly with the time of the recording from the value before insertion to the one measured at the end of the last ischemia/reperfusion cycle.

The needle array was positioned on the anterior left ventricle and left ventricular free wall with the posterior surface of

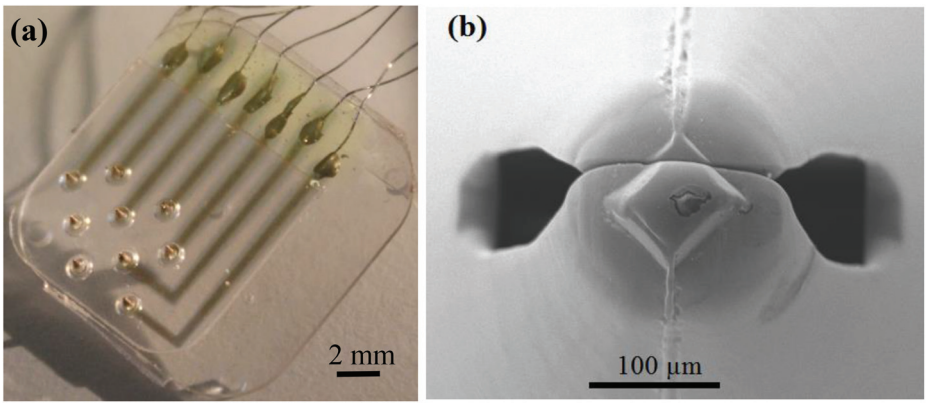

Fig. 1 (a) Distribution pattern of the microneedle array and (b) detail of the needle tip by SEM microscopy (accelerating voltage 20 kV, 250×).

Table 1 Average values (Av.) of the slope and offset with the related standard deviation, σ, as calculated from the linear regression carried out from the calibration of the microneedle arrays. Each device consists of 7 IrOx-coated individually addressable needles and the table reports the intra-batch (n = 7) and inter-batch calibration (n = 14) values. IrOx was deposited from the plating solution by applying a potential equal to 0.835 V (arrays A and B), 0.935 V (arrays C and D) and 1.035 V (arrays E and F). Δ% represents the percentage change of the calibration values compared to day 1

	Array A		Array B		Inter-batch			
Day	Av.	σ	Av.	σ	Av.	σ	$-\Delta$%	
1	75.4	0.4	74.4	0.3	74.9	0.7	—	Slope
3	69.0	0.7	67.7	0.3	68.3	0.9	8.8	
5	67.2	1.2	65.7	0.4	66.4	1.2	11.3	
1	750.5	9.9	730.0	8.0	740.3	13.7	—	Offset
3	610.4	15.6	579.4	4.2	594.9	19.5	19.6	
5	541.2	16.1	537.1	5.2	539.1	11.7	27.2	
	Array C		Array D		Inter-batch			
Day	Av.	σ	Av.	σ	Av.	σ	$-\Delta$%	
1	75.6	0.7	73.9	0.5	74.7	1.1	—	Slope
3	68.1	1.1	67.2	0.5	67.7	1.0	9.5	
5	65.4	0.9	65.7	0.4	65.5	0.7	12.4	
1	768.6	13.3	730.9	8.9	749.8	22.4	—	Offset
3	605.6	14.6	571.3	6.5	588.4	20.9	21.5	
5	536.5	13.2	542.0	6.5	539.3	10.4	28.1	
	Array E		Array F		Inter-batch			
Day	Av.	σ	Av.	σ	Av.	σ	$-\Delta$%	
1	71.7	1.3	70.7	2.3	71.2	1.8	—	Slope
3	65.8	6.8	65.6	2.1	65.7	4.9	7.7	
5	61.4	6.9	63.9	1.6	62.7	5.0	12.0	
1	690.5	15.4	717.5	17.1	704.0	21.0	—	Offset
3	606.4	51.9	578.3	28.8	592.4	42.9	15.9	
5	470.6	185.8	536.7	11.4	503.7	131.0	28.5	

the heart supported by pins. With the tip of the inserter resting on the back of the platform, the spring mechanism controlling the piston of the inserter was triggered thus pushing the needles into the tissue. This part of the procedure was repeated twice or thrice to fully secure the spikes into the myocardium wall. After 8–10 minute stabilization the heart underwent cycles of global no-flow ischemia (15 minutes) followed by reperfusion (15 minutes) with continuous pH monitoring. In order to follow the depth of the electrode spikes, the hearts were processed histologically. Following the excision of the organ, the heart was fixed in formalin, then frozen and sliced in the cryostat in 90 μm sections. The sections were stained using Nissl preparation before microscope investigation.

Results and discussion

Fig. 1a and b show the pattern of microneedles in the array employed in this investigation and the detail of the microneedle tip, respectively. The needles are arranged in a equilateral triangular pattern and the distances (center-to-center) among them is *ca.* 2.2 mm. This spatial arrangement allows mapping pH heterogeneities across a significant proportion of the ventricular myocardium. It should be noted that this specific pattern was chosen for convenience in the manufacture process rather than for physiological considerations. The radius and height of the needles are *ca.* 0.8 mm and 1.6 mm, respectively, and the tip diameter at the apex is 50–80 μm. It is important to note that the thickness of the myocardium is 2–3 mm.[42] Fig. S2a† reports the typical cyclic voltammograms obtained with the microneedle array platform immersed in the IrOx plating solution. Fig. S2b† compares the voltammograms of IrOx-coated and gold needles obtained in 0.5 M H_2SO_4. Overall these results suggested the formation of a defect-free iridium oxide coating and agree with previous findings.[18,43]

Fig. S3 in the ESI† provides an example of a typical calibration curve of an array of IrOx-coated needles. It is important to note that all the sensors have a linear response in the pH window from 4 to 8 independent of the deposition potential (see Tables S1–S3 in the ESI†). Table 1 summarizes the average values of the slope and offset of the calibration obtained with sensors prepared by plating IrOx at 0.835, 0.935 and 1.035 V *vs.* SCE. The initial values of the offset (inter-batch average) are 740.3 ± 13.7, 749.8 ± 22.4 and 704.0 ± 21.0, respectively, and the values of the slope (inter-batch average) are 74.9 ± 0.7, 74.7 ± 1.1, and 71.2 ± 1.8, respectively.

Table 1 reports also the changes in the calibration trends upon dry-storage of the microneedle sensors. Slope and offset values diminish over time, however, the response of the sensors remains linear upon storage (R^2 values always larger than 0.996) thus suggesting that the sensor characteristics can be tested using a two-point calibration. The hourly-drift of the sensors is equivalent to a displacement of pH units equal to −0.02 ± 0.01 (n = 7) and −0.03 ± 0.02 (n = 6) as evaluated by measuring the potential of the sensors immersed in a phosphate buffer (pH = 6.80 ± 0.05) containing 0.1 M KNO_3 or 0.1 M KCl, respectively. Interestingly, in de-oxygenated buffer the drift reverses and corresponds to a displacement of 0.03 ± 0.01 pH units per hour (n = 7), see Fig. S4a in the ESI.† These results suggest that the etching of the IrOx layers in the presence of Cl^- ions[18,43] is not particularly severe and that the sensors are suitable for long-term monitoring of pH with good accuracy.

It is important to quantify possible sources of interferents also in relation to the chemicals ($MgCl_2$, $CaCl_2$, glucose) of the perfusate buffer employed for the *ex vivo* preparations. Fig. 2a displays traces of the potential of the sensors upon spiking a phosphate buffer solution (pH = 6.80 ± 0.05) containing 0.1 M KCl with $CaCl_2$ and $MgCl_2$ at the times indicated by the arrows. Similar trends were obtained by replacing 0.1 M KCl with 0.1 M KNO_3 as a background electrolyte, although the displacements of the potential of the sensors were smaller in the latter case (not shown). A reverse trend can be observed in the figure, *i.e.*, first, second and third additions of $CaCl_2$ produced a change of *ca.* −1, 0 and 4 mV, respectively. In contrast, the

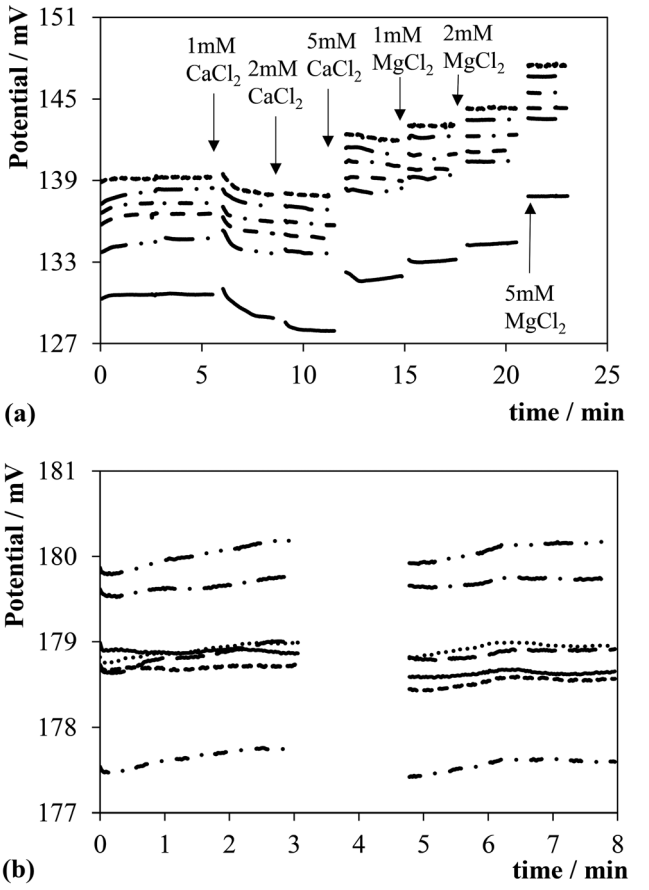

Fig. 2 Each line represents the individual trace of the ΔE of six IrOx-coated needles immersed in a phosphate buffer (pH = 6.80 ± 0.05) containing (a) 0.1 M KCl or (b) 0.1 M KNO_3. (a) The buffer was spiked with 0.4 M aqueous $CaCl_2$ and 0.4 M aqueous $MgCl_2$ at the time indicated by the arrows and the resulting concentrations of $CaCl_2$ and $MgCl_2$ are reported in the graph. (b) Albumin was added at t = 3 min in order to obtain a final concentration of 1 g L^{-1} and after 2 minutes of stirring without recording the measurements were then re-started under quiescent conditions.

following additions of $MgCl_2$ produced an increase in the potential of ~1 mV for each millimolar concentration increase. The reverse trend observed during the additions of $CaCl_2$ is not fully understood, however, there is evidence for the involvement of ions in equilibrium reactions in Ir oxide films.[24,25] These results highlight a slight sensitivity to $CaCl_2$ and $MgCl_2$, however, at worst this is equivalent to an error of pH units of -0.12 ± 0.01 ($n = 6$). Fig. 2b provides evidence that the sensors are not susceptible to albumin at least for concentrations below 1 g L^{-1} since the traces of the potential are almost unaffected, *i.e.*, the displacement of the potential is below 1 mV. It is also important to note that glucose does not impact on the pH readings as shown in Fig. S4b in the ESI.†

Fig. 3a reports an indentation in the cardiac tissue caused by the insertion of a microneedle. This indentation has an arrow shape and the characteristic dimensions are *ca.* 0.30 mm and 0.25 mm, corresponding to the depth and base of the triangular part, respectively. The overall morphology resembles the shape of the microneedle and the mismatch in dimensions arises probably from the shrinkage of cardiac tissue during the histopathology procedure. The final device was tested during a heart ischemia/reperfusion experiment in order to prove its suitability for mapping the organ pH distribution. Fig. 3b demonstrates that the recorded electrocardiograms before and after needle array impalement were unchanged. In fact, there were no significant changes to the heart rate, QRS complex morphology or the ST segment/T wave, all indicating that the impalement of the microneedles did not produce detectable local myocardial injuries or affect the electrophysiology of the heart. Fig. 4 shows a device inserted into an *ex vivo* perfused rat heart and the video in the ESI† demonstrates that the inserted platform moves alongside the beating heart.

It is important to note that not all the needles penetrated the myocardium wall because of the shape and dimension of the heart in comparison with the device. For instance, the needles in Fig. 4a were divided into 3 groups upon

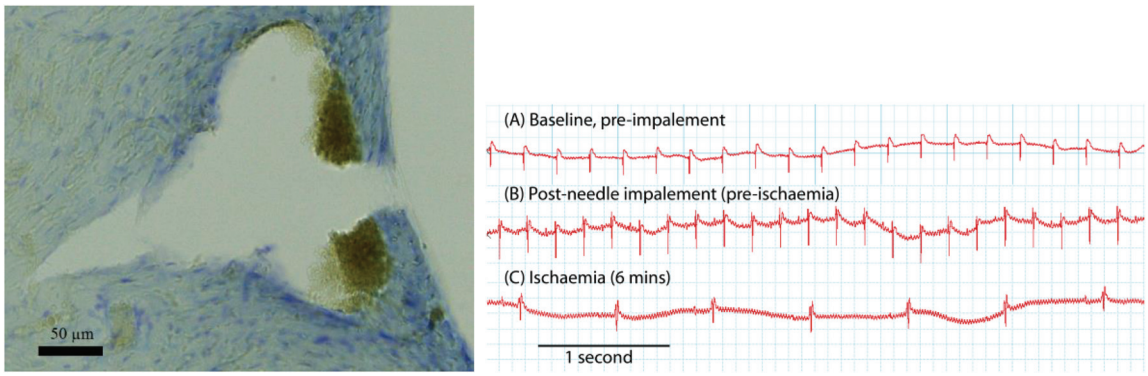

Fig. 3 (a) The imprint of a microneedle after insertion into the heart tissue and following histopathology treatment as specified in the Experimental section. The image was acquired using a 20× magnification. (b) Comparison between electrograms recorded before and after impalement of the microneedle array into the myocardium and during global no-flow ischemia with the pH sensing device inserted into the heart.

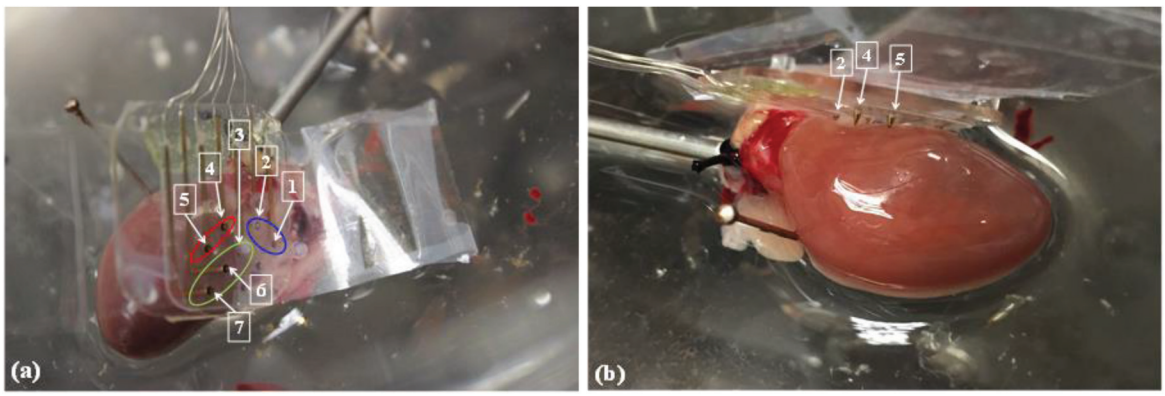

Fig. 4 IrOx-coated microneedle array inserted into the explanted rat heart which is bathing in Tyrode's solution. Pictures show the device (a) from top (the visible dark disks correspond to the back of the needles) and (b) from the side. Needles were divided into three groups upon visual inspection: needles well inserted into the myocardium, group i, which are circled with a green (—) line; well inserted into a fatty area, group ii, circled with a blue (—) line; and needles with the tip resting on the pericardium, group iii, circled with a red (—) line.

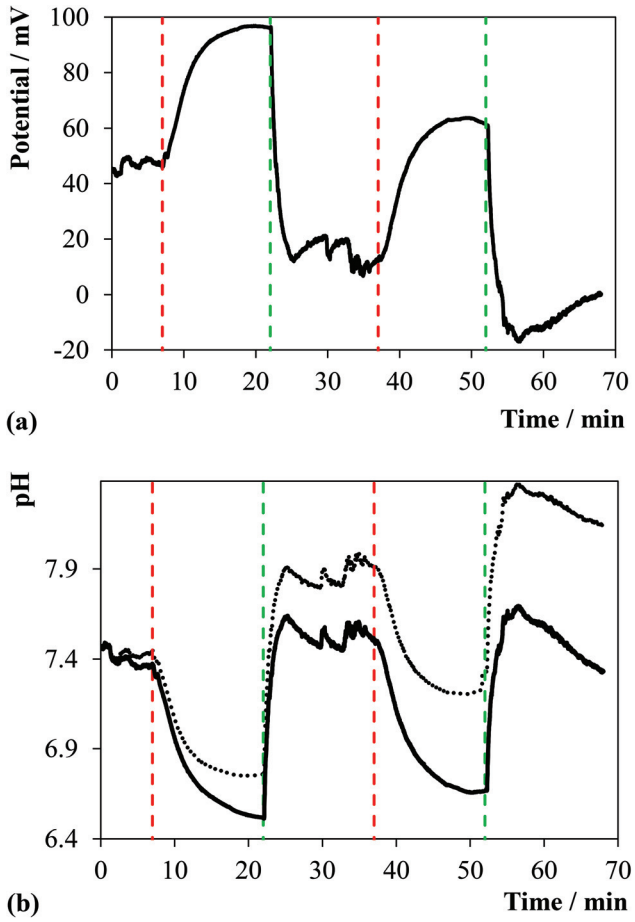

Fig. 5 Traces of the (a) potential and (b) pH (derived from the former) as measured by a microneedle inserted into an *ex vivo* perfused rat heart. The latter figure compares pH trends with (—) and without (···) drift correction. After 7 minutes background recording, the rat heart underwent two cycles of global heart ischemia/reperfusion. Ischemia occurred at 8 and 38 minutes while reperfusion started at 22 and 52 minutes as indicated by the red and green dashed vertical lines, respectively.

visual inspection: (i) well inserted into the myocardium, (ii) well inserted in a region of fatty tissue, and (iii) tip of the needle in contact with the pericardium. Fig. 5a presents an example of the traces of the potential obtained with one of the spikes belonging to group i. Fig. 5b compares the pH trend calculated from the value of potential bias with and without drift correction. It can be noted that the drift caused by biofouling is noteworthy by corresponding to an average of 47.2 ± 12.4 mV shift (n = 7) as measured by comparing the ΔE of the sensors in the same buffer before and after the cardiac pH mapping. Fig. S5 in the ESI† compares the traces of pH obtained with the remaining sensors of the array.

It is significant to note that the pH as measured by the sensors in group i and ii is stable during the initial 8 minutes baseline recording, *ca.* 7.3, while the pH of the sensors in group iii moves upwards. This result may be a mechanical artefact since only the tip of the sensors of this group is in contact with the pericardium, *i.e.*, likely to be susceptible to movements produced by the beating heart, however, other factors such as the drying out of the pericardium may have some impact on these pH readings. More significantly, stopping the coronary perfusion causes an immediate drop in the pH concurrent to the establishing of an acidotic environment. As soon as the flow of perfusate re-starts the pH increases towards the initial values with faster dynamics compared to the ischemic event as previously observed.[27] A spatio-temporal map of the pH distribution in the cardiac tissue was constructed using the pH data obtained from the individual needles, see Fig. 6. The figure provides a visual of the real-time pH microenvironments existing across the whole heart during ischemia/reperfusion cycles. This result, thus, confirms the potential of the microneedle array here reported for mapping pH distribution in biological samples such as organs and its usefulness as a bioanalytical tool for direct pH measurements.

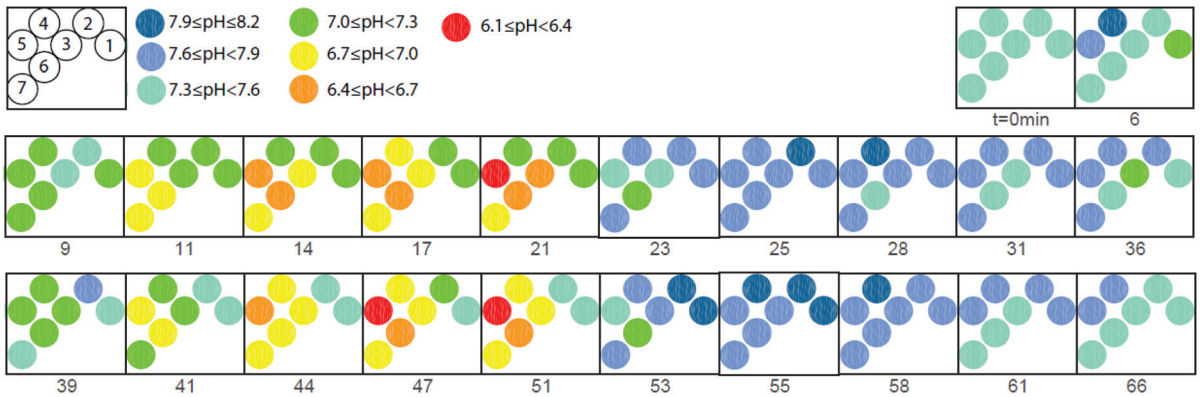

Fig. 6 Colour map of the pH distribution obtained with the microneedle device inserted into an *ex vivo* perfused rat heart. The map reports the snapshots of the pH measured by the sensors at the minutes indicated below each frame. Each labelled disk represents a microneedle and the colour legend for the pH ranges is given in the figure. After 7 minutes background recording, the rat heart underwent two cycles of global heart ischemia/reperfusion. Ischemia occurred at t = 8 min and 38 min while reperfusion started at t = 22 min and 52 min.

Conclusions

An array of individually addressable pH sensitive needles was prepared, optimized and tested during bench and *ex vivo* experiments. A deposition potential smaller than 0.935 V *vs.* SCE was found optimal to minimize the intra- and inter-batch reproducibility. The investigation highlighted that the sensor calibration parameters changed over a period of 5 days after preparation although retaining a linear response within the pH window between 4 and 8. This device was tested on an explanted heart undergoing cycles of global ischemia/reperfusion allowing mapping the pH distribution across multiple sites of the heart and showing the regional dynamics of the ischemic response.

Acknowledgements

This work was supported by the European Research Council (Synergy Grant No. 319818, i2MOVE). We would like to thank the FILM facilities at the Imperial College for their help, support and assistance. Fu Siong Ng was supported by an NIHR Clinical Lectureship (1716) and an Academy of Medical Sciences Starter Grant (AMS-SGCL8-Ng).

References

1 L. M. Strambini, A. Longo, A. Diligenti and G. Barillaro, *Lab Chip*, 2012, **12**, 3370–3379.
2 J. J. Norman, S.-O. O. Choi, N. T. Tong, A. R. Aiyar, S. R. Patel, M. R. Prausnitz and M. G. Allen, *Biomed. Microdevices*, 2013, **15**, 203–210.
3 U. O. Häfeli, A. Mokhtari, D. Liepmann and B. Stoeber, *Biomed. Microdevices*, 2009, **11**, 943–950.
4 E. V. Mukerjee, S. D. Collins, R. R. Isseroff and R. L. Smith, *Sens. Actuators, A*, 2004, **83**, 231–236.
5 K. Ajeet, V. Abhay, K. A. Sunil, P. Syed Khalid and B. Shekhar, *Biosens. Bioelectron.*, 2013, **53**, 499–512.
6 P. Vazquez, G. Herzog, C. O'Mahony, J. O'Brien, J. Scully, A. Blake, C. O'Mathuna and P. Galvin, *Sens. Actuators, B*, 2014, **201**, 572–578.
7 K. Do Hee, J. Ho Sang, W. Taejun, S. Myeong Hwan, K. Young-Eun, K. Ki Hean, A. G-One and H. Sei Kwang, *Adv. Healthcare Mater.*, 2015, **4**, 1153–1158.
8 G. Valdés-Ramírez, Y.-C. Li, J. Kim, W. Jia, A. J. Bandodkar, R. Nuñez-Flores, R. P. Miller, S.-Y. Wu, R. Narayan, J. R. Windmiller, R. Polsky and J. Wang, *Electrochem. Commun.*, 2014, **47**, 58–62.
9 P. M. Wang, M. Cornwell and M. R. Prausnitz, *Diabetes Technol. Ther.*, 2005, **7**, 131–141.
10 P. R. Miller, X. Xiao, I. Brener, D. B. Burckel, R. Narayan and R. Polsky, *Adv. Healthcare Mater.*, 2014, **3**, 876–881.
11 J.-H. H. Lee, Y. Seo, T.-S. S. Lim, P. L. Bishop and I. Papautsky, *Environ. Sci. Technol.*, 2007, **41**, 7857–7863.
12 S. D. Gittard, A. Ovsianikov, B. N. Chichkov, A. Doraiswamy and R. J. Narayan, *Expert Opin. Drug Delivery*, 2010, **7**, 513–533.
13 A. Jina, M. J. Tierney, J. A. Tamada, S. McGill, S. Desai, B. Chua, A. Chang and M. Christiansen, *J. Diabetes Sci. Technol.*, 2014, **8**, 483–487.
14 M. A. Invernale, B. C. Tang, R. L. York, L. Le, D. Y. Hou and D. G. Anderson, *Adv. Healthcare Mater.*, 2014, **3**, 338–342.
15 J. R. Windmiller, G. Valdés-Ramírez, N. Zhou, M. Zhou, P. R. Miller, C. Jin, S. M. Brozik, R. Polsky, E. Katz, R. Narayan and J. Wang, *Electroanalysis*, 2011, **2011**, 2302–2309.
16 Z. Hongbo, L. Gang, S. Xiaona, Z. Zhuanghui, X. Baojian, J. Qinghui, Z. Jianlong and R. Qiu-Shi, *Sens. Actuators, A*, 2009, **150**, 150.
17 Y.-K. Yoon, J.-H. Park and M. G. Allen, *J. Microelectromech. Syst.*, 2006, **15**, 1121–1130.
18 S. R. Ng and D. O'Hare, *Analyst*, 2015, **140**, 4224–4231.
19 C. Zuliani, G. Matzeu and D. Diamond, *Electrochim. Acta*, 2014, **132**, 292–296.
20 C. Zuliani and D. Diamond, *Electrochim. Acta*, 2012, **84**, 29–34.
21 C. Zuliani, V. F. Curto, G. Matzeu, K. J. Fraser and D. Diamond, in *Comprehensive Materials Processing*, ed. S. Hashmi, Elsevier Science & Technology Books, 2014, pp. 221–243.
22 S. Anastasova, A. M. Spehar-Deleze and P. Vadgama, in *Sensors, Actuators, and Microsystems*, ed. M. Carter, Z. Aguilar, B. Ward and J. Li, 2012, pp. 43–48.
23 S. Anastasova, A.-M. Spehar-Deleze, D. Bickham, P. Uebel, M. Schmidt, P. Russell and P. Vadgama, *Electroanalysis*, 2012, **24**, 529–538.
24 P. Steegstra and E. Ahlberg, *Electrochim. Acta*, 2012, **76**, 26–33.
25 P. Steegstra and E. Ahlberg, *Electrochim. Acta*, 2012, **68**, 206–213.
26 A. N. Bezbaruah and T. C. Zhang, *Anal. Chem.*, 2002, **74**, 5726–5733.
27 H.-J. J. Chung, M. S. Sulkin, J.-S. S. Kim, C. Goudeseune, H.-Y. Y. Chao, J. W. Song, S. Y. Yang, Y.-Y. Y. Hsu, R. Ghaffari, I. R. Efimov and J. A. Rogers, *Adv. Healthcare Mater.*, 2014, **3**, 59–68.
28 S. A. Marzouk, R. P. Buck, L. A. Dunlap, T. A. Johnson and W. E. Cascio, *Anal. Biochem.*, 2002, **308**, 52–60.
29 G. X. Yan and A. G. Kleber, *Circ. Res.*, 1992, **71**, 460–470.
30 I. Bogachan Tahirbegi, M. Mir, S. Schostek, M. Schurr and J. Samitier, *Biosens. Bioelectron.*, 2014, **61**, 124–130.
31 V. V. Cosofret, M. Erdosy, T. A. Johnson, R. P. Buck, R. B. Ash and M. R. Neuman, *Anal. Chem.*, 1995, **67**, 1647–1653.
32 S. R. Gutbrod, M. S. Sulkin, J. A. Rogers and I. R. Efimov, *Prog. Biophys. Mol. Biol.*, 2014, 115.
33 E. C. Keeley, J. A. Boura and C. L. Grines, *Lancet*, 2003, **361**, 13–20.
34 H. R. Cross, E. Murphy and C. Steenbergen, *Am. J. Physiol.*, 2002, **283**, H481–H489.
35 D. Feuvray, *Cardiovasc. Res.*, 1997, **34**, 48–54.

36 S. Sanada, I. Komuro and M. Kitakaze, *Am. J. Physiol.*, 2011, **301**, H1723–H1741.
37 D. M. Yellon and D. J. Hausenloy, *N. Engl. J. Med.*, 2007, **357**, 2409–2410.
38 G. M. C. Rosano, M. Fini, G. Caminiti and G. Barbaro, *Curr. Pharm. Des.*, 2008, **14**, 2551–2562.
39 L. Xu, S. R. Gutbrod, A. P. Bonifas, Y. Su and M. S. Sulkin, *Nat. Commun.*, 2014, **5**, 3329–3329.
40 W.-H. Choi and I. Papautsky, *J. Micro/Nanolithogr., MEMS, MOEMS*, 2011, **10**, 020501.
41 S. C. Mailley, M. Hyland, P. Mailley, J. M. McLaughlin and E. T. McAdams, *Mater. Sci. Eng., C*, 2002, **21**, 167–175.
42 R. M. McAdams, R. J. McPherson, N. M. Dabestani, C. A. Gleason and S. E. Juul, *Comp. Med.*, 2011, **61**, 12–12.
43 M. L. Hitchman and S. Ramanathan, *Analyst*, 1988, **113**, 35–39.